Applied Catalysis B: Environmental 162 (2015) 310–318

Contents lists available at ScienceDirect

Applied Catalysis B: Environmental

journal homepage: www.elsevier.com/locate/apcatb

Nitrogen-doped, metal-modified rutile titanium dioxide as photocatalysts for water remediation

D. Dolat[a,*], S. Mozia[a], R.J. Wróbel[a], D. Moszyński[a], B. Ohtani[b], N. Guskos[c], A.W. Morawski[a]

[a] Institute of Chemical and Environment Engineering, West Pomeranian University of Technology, Szczecin, ul. Pułaskiego 10, 70-310 Szczecin, Poland
[b] Catalysis Research Center, Hokkaido University, Sapporo 001-0021, Japan
[c] Institute of Physics, West Pomeranian University of Technology, Szczecin, Al. Piastów 48, 70-311 Szczecin, Poland

ARTICLE INFO

Article history:
Received 11 February 2014
Received in revised form 26 June 2014
Accepted 1 July 2014
Available online 8 July 2014

Keywords:
Photocatalysis
Rutile-TiO_2
co-modification

ABSTRACT

A comparison study of metal (Fe, Co, or Ni) – modification, nitrogen – doping of rutile titanium dioxide via impregnation followed by calcination method is presented. The aim of this study was to obtain a highly photoactive rutile titanium dioxide and to establish the origin of its photoactivity with reference to the influence of the physicochemical properties of the modified materials and the type of the applied metal. Moreover, the properties of the co-modified photocatalysts were compared to those of the single (metal or nitrogen) modified materials. For this purpose highly advanced analytical methods such as SEM with EDS, XPS, EPR–AFMR, XRD, ICP–OES, UV–vis/DR, N_2 adsorption/desorption at 77 K and elemental analysis were employed. We have proved that a proper modification of rutile may lead to obtaining highly visible and/or UV light active materials. It has been revealed that the metal applied for rutile titanium dioxide modification plays a crucial role in its photocatalytic performance. In case of visible light the Fe > Ni > Co order and in case of UV light activity the Ni > Fe > Co order, for both single-modified and co-modified materials, is followed. Moreover, it was proven that the co-modified samples exhibited significantly higher activity than the single-modified rutile. An effort has been made in order to shed light on this new, unexplored area of titanium dioxide modification and application.

1. Introduction

Titanium dioxide is undoubtedly the most studied semiconductor for photocatalytic water and air remediation due to its high stability, fine optical properties and availability [1,2]. Nevertheless, despite many advantages of this material, its commercial application is still limited. The main obstacles to be overcome before titanium dioxide can be successfully used for solar light applications are: (1) Wide band gap of 3.2 eV and 3.0 eV for anatase and rutile TiO_2, respectively, which implies application of, additionally to solar, UV light irradiation source [3,4]; (2) Rapid electron–hole pairs recombination [5,6] resulting in low electron concentration in conduction band of TiO_2, which diminishes the photocatalytic efficiency of the semiconductor [7].

In order to overcome these difficulties the researchers employed numerous modification methods among which the non-metal doping [8,9] as well as transition metal-doping [10] seem to be the most promising for TiO_2 band-gap narrowing, whereas titanium dioxide modification with metals [11], graphene [12,13] or semiconductors coupling [14,15] are mainly used in order to inhibit electron/hole pairs recombination rate. Among non-metals, it is nitrogen, which attracts the most attention. Starting from the paper by Asahi et al. [16], every year numerous publications considering this subject are published [17]. The significantly higher interest in nitrogen in regard to other non-metals arises from the fact that nitrogen can be relatively easily incorporated in TiO_2 structure [18]. Moreover, the position of newly formed, after nitrogen-doping, energy state above the valence band of TiO_2 possesses sufficiently high oxidation potential for water contaminants photodegradation [19] which is not always the case for carbon, sulfur or fluorine-doped TiO_2 [17]. Theoretical studies discuss different influence of titanium dioxide N-doping on anatase and rutile form of TiO_2 [20]. Di Valentin et al. [21] claim that whereas the position of the valence band of N-doped anatase increases by 0.14 eV or 0.73 eV for substitutional and interstitial doping, respectively, the valence band position of N-doped rutile decreases by 0.03 eV and the position of the rutile conduction band increases by 0.05 eV, resulting in higher band gap energy than for pure rutile (3.08 eV for N-doped vs. 3.0 eV

* Corresponding author. Tel.: +0048914494277; fax: +0048914494686.
E-mail addresses: ddolat@zut.edu.pl, dianadolat@wp.pl (D. Dolat).

http://dx.doi.org/10.1016/j.apcatb.2014.07.001
0926-3373/

for pure rutile). Although, to the best of our knowledge, there is no experimental work available to confirm this statement, it cannot be neglected.

Surface metal modification of titanium dioxide may increase the photocatalytic efficiency of the material by working as the so called co-catalysts, which induce electron transport from TiO_2 conduction band to the metal/semiconductor inter-phase thus inhibiting electron/hole recombination rate [22–24]. Creutz et al. [22] studied photocatalytic activity of Ti^{3+} doped titanium dioxide. The photocatalyst was inactive even under UV light irradiation. Only after its surface modification with copper(II) or iron(III), which significantly increased charge separation, the photocatalytic activity of TiO_2 increased dramatically. Liu et al. [25] obtained visible light active materials by simultaneous doping and surface modification of TiO_2 using iron ions. Doped-iron allowed successful absorption of visible light fraction whereas iron grafted on the TiO_2 surface increased quantum efficiency by allowing effective separation of photo-generated electron–hole pairs.

In our previous work [26,27] we have discussed the possibility of obtaining visible light active rutile-TiO_2 photocatalysts by the nitrogen-doping and metal (Me = Fe or Ni) modification. The obtained results were very promising. In this study, we describe nitrogen-doped cobalt-modified rutile titanium dioxide and compare it to our earlier works, focusing on the cobalt modification and referring to the materials from the previous publications. Moreover, in this paper we provide some new information about the earlier described materials and focus on the origin of the visible and UV light activity of rutile-TiO_2 photocatalysts.

2. Experimental

2.1. Materials

Commercial P25 TiO_2 (Evonik, Germany) with BET surface area of 55.5 $m^2\,g^{-1}$ and commercial rutile (Catalysis Society, Japan) with BET surface area of 100 $m^2\,g^{-1}$ were used as reference photocatalysts. Water suspension of crude, industrial grade titanium dioxide (TiO_2/A), consisting of water, TiO_2 (ca. 35 wt.%, including amorphous, anatase and rutile at the ratio of 61.5:35:3.5), and residual sulfuric acid (ca. 8 wt.% in regard to TiO_2 content, from sulfate technology) supplied by Chemical Factory "Police" S.A. (Poland) with BET surface area of 238 $m^2\,g^{-1}$ was used as a pristine material for the synthesis of modified TiO_2. Metal nitrates ($Fe(NO_3)_3{\cdot}9H_2O$, $Co(NO_3)_2{\cdot}6H_2O$, $Ni(NO_3)_2{\cdot}6H_2O$) and ammonia were used as metal and nitrogen precursors, respectively. A model solution of acetic acid (5 vol.%) was applied in order to evaluate the photocatalysts' activity. High purity water for the photocatalytic experiments and sample analysis was produced by a Millipore Elix Advantage water purification system that provides bacteria free water at 18 $M\Omega\,cm^{-1}$, resistivity, and with less than 1 ppb total organic carbon.

2.2. Nitrogen doping, metal modification and metal, nitrogen co-modification procedure

The TiO_2 modification was conducted according to the procedure described in our previous publications [26,27]. Water suspension of an industrial grade amorphous titanium dioxide (TiO_2/A) from sulfate technology supplied by "Chemical Factory Police S.A." (Poland) was used as a starting material. About 20 g of TiO_2/A was introduced into a beaker containing aqueous solution of $Me(NO_3)_2{\cdot}xH_2O$ (used as a source of iron, cobalt or nickel) and stirred for 48 h. The amount of metal nitrate introduced to the beaker was of 5 wt.% relatively to TiO_2 content. After water evaporation, the samples were dried at 80 °C for 24 h in an oven. Subsequently, the materials were calcined for 4 h at 800 °C in either Ar flow (Me-modified samples denoted as Me–TiO_2/R, where Me = Fe, Co or Ni) or NH_3 (Messer, 99.85%) flow (co-modified samples denoted as Me,N–TiO_2/R). NH_3 was used as nitrogen and hydrogen source. Additionally, for comparison purpose, N–TiO_2/R was prepared without $Me(NO_3)_2$ impregnation step.

2.3. Photocatalysts' characterization

The photocatalysts' light absorption abilities were characterized by means of UV–vis/DR technique using Jasco V-650 spectrophotometer (Japan) equipped with an integrating sphere accessory for diffuse reflectance spectra acquisition (Spectralon was used as a reference). The crystalline structure of the photocatalysts was characterized by X-ray powder diffraction (XRD) analysis (X'Pert PRO Philips diffractometer) using Cu $K\alpha$ radiation. The specific surface area (S_{BET}) of the photocatalysts was determined on a basis of N_2 adsorption at 77 K using Quadrasorb SI (Quantachrome Instruments, U.S.A.) instrument. Prior to analyses, each sample was degassed at 105 °C for 24 h under high vacuum. The values of the S_{BET} were determined using multi-point analysis of adsorption isotherms applying Brunauer–Emmett–Teller (BET) equation. The X-ray photoelectron spectra (XPS) were obtained using Mg $K\alpha$ ($h\nu$ = 1253.6 eV) radiation for the samples containing iron and cobalt additives, while the sample with nickel addition was studied with use of Al $K\alpha$ ($h\nu$ = 1486.6 eV) radiation. Scienta SES 2002 spectrometer operating at constant transmission energy (E_p = 50 eV) was used to acquire the spectra. The samples were also analyzed with application of scanning electron microscopy with cold emission SEM SU8020 (Hitachi, Japan) coupled with energy-dispersive X-ray spectroscopy (SEM-EDS, EDS NSS 312, Thermo Scientific) allowing elemental microanalysis. Total nitrogen content in the samples was determined with application of Leco ONH836 elemental analyzer. The concentration of metals in the samples was determined by ICP–OES method using Perkin Elmer Optima 5300 DV spectrometer. Prior to these analyses the photocatalysts were diluted in a hot H_2SO_4 with addition of water and HCl.

2.4. Photoactivity evaluation method

The photocatalytic activity of all new materials as well as commercial photocatalysts for comparison purpose was determined on the basis of CO_2 evolution rate during oxidative decomposition of acetic acid. The evaluation of photoactivity of the different synthesized materials was conducted at a constant volumetric rate of photon absorption (VRPA) by providing photocatalyst concentration conditions which allowed all the light induced to be absorbed by the slurry. This method allows the evaluation of the intrinsic photoactivity of each material [28]. The procedure was conducted under irradiation using mercury lamp emitting wavelengths >290 nm. For visible light tests a cut-off optical filter providing irradiation wavelengths longer than 400 nm was applied.

3. Results and discussion

3.1. Crystal Structure

Fig. 1 presents XRD patterns of the cobalt-modified and cobalt, nitrogen co-modified rutile titanium dioxide materials together with the starting material (TiO_2/A). (The XRD patterns of all the other samples are available in our previous publications [26,27] as well as in Supplementary information—S1). According to XRD measurements all metal-modified photocatalysts (Me–TiO_2/R) consisted of two phases: rutile TiO_2 and ternary oxide, namely $TiFe_2O_5$, $CoTiO_3$ and $NiTiO_3$ for iron, cobalt and nickel modification, respectively. The mixed oxides are also semiconductors and

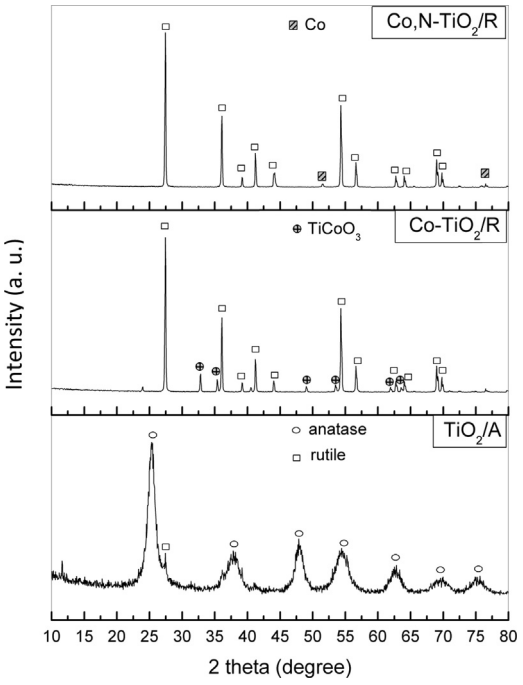

Fig. 1. XRD patterns of Co-modified rutile TiO_2 and TiO_2/A.

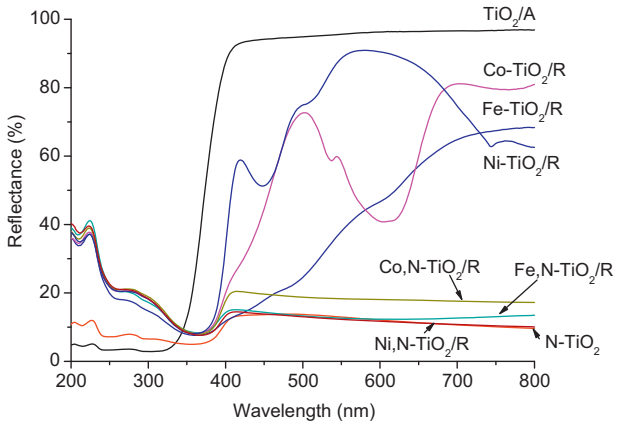

Fig. 2. UV–Vis/DR spectra of Me-modified rutile-TiO_2, Me, N-co-modified rutile-TiO_2 as well as amorphous TiO_2/A.

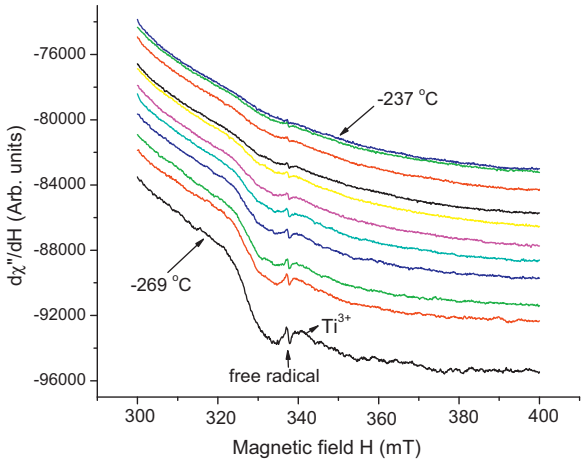

Fig. 3. Temperature dependence of the EPR spectra for Co,N–TiO_2/R sample.

their band gaps energies are of about 2.2 eV, 2.25 eV and 2.16 eV for $TiFe_2O_5$, $CoTiO_3$ and $NiTiO_3$, respectively [29]. The low band gap energy allows these materials to absorb wider spectrum of visible light irradiation than titanium dioxide, but, as it is typical for oxide semiconductors with narrow band-gap, they are photocatalytically inactive due to rapid electron/hole pairs recombination, which suppresses the charge transfer and as a consequence surface redox reaction with adsorbed species [30]. In the literature, there are available publications discussing possibility of coupling titanium dioxide with $TiFe_2O_5$, $CoTiO_3$ or $NiTiO_3$, for better charge separation [31,32] since the described semiconductors coupled systems absorb light from a wide spectrum of solar irradiation, even up to 575 nm. The co-modified samples (Me,N–TiO_2/R) consist also mainly of rutile phase and small amounts of $TiFeO_3$, Co and Ni, respectivley. Further investigation of Co and Ni presence in these samples will be provided later.

3.2. Optical and Magnetic Properties

An extended light absorption of all Me-modified TiO_2 towards longer wavelength can be seen in Fig. 2 due to the presence of ternary metal oxides in these materials. At the same time very strong and stable light absorption even up to 800 nm can be noticed for all the co-modified materials. These strong light absorption properties of co-modified samples derived most likely from the presence of titanium trivalent ions (Ti^{3+}) and/or accompanying oxygen vacancies in the samples, resulting in a black color of these materials [34,35]. However, although the concentration of Ti^{3+} ions in Ni,N–TiO_2/R and Fe,N–TiO_2/R materials was significant (EPR spectra of these samples are shown in Supplementary Information—S2 and S3) in case of Co,N–TiO_2/R the trivalent titanium ions were not detected by EPR method until the temperature was lowered to −269 °C (cf. Fig. 3). Weak signal of trivalent titanium ions which can only be bserved at very low temperatures suggests low concentration of these species in the materials' structure. In case of nickel, nitrogen and iron, nitrogen co-modified samples, where trivalent titanium ions could form new energy levels, accessible for electrons below the minimum of the conduction band of TiO_2, which could lead to an increase in the visible light absorption and photocatalytic performance of the new materials. On the contrary, in case of the cobalt, nitrogen co-modified rutile the presence of only small amounts of Ti^{3+} ions may cause a decrease of the photocatalytic performance of this material. It was earlier reported by Weidmann et al. [36] that low concentration of trivalent titanium ions in titania structure may serve as electrons/holes recombination centers, thus decreasing the charge density and therefore photocatalytic activity of the materials.

3.3. Surface Content Based on XPS and Morphology

X-ray photoelectron spectroscopy was utilized to determine the character of the chemical bonds present in the studied materials. The position of the maximum of XPS Ti $2p_{3/2}$ peak was 458.7 ± 0.1 eV for samples containing iron and cobalt additives (Fig. 4). This indicates that titanium atoms are in form of Ti^{4+} cations surrounded by oxygen atoms as in TiO_2 [37–39]. In case of the sample denoted Ni,N–TiO_2/R the maximum is slightly shifted to the position of 458.5 eV and has very similar profile to Ti 2p spectrum previously observed for nitrogen-modified TiO_2, discussed in detail in the previous paper [40]. The results suggest that nitrogen atoms were incorporated into TiO_2 in the Ni,N–TiO_2 sample where apart from TiO_2 some contribution of TiN and TiON species are supposed to be present.

In Fig. 4b) the region characteristic for XPS N 1s peak is presented for the three Me,N–TiO_2/R samples containing nickel, iron or cobalt compound admixture, respectively. Only in case of the

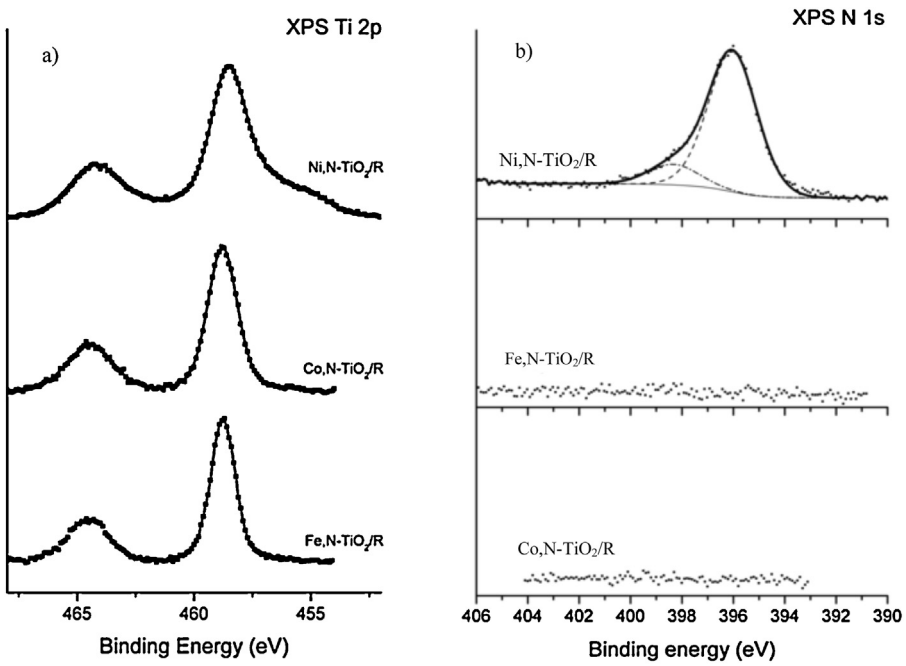

Fig. 4. The XPS spectra of a) Ti $2p_{3/2}$ lines and b) N 1s lines for Me,N–TiO_2/R photocatalysts.

Ni,N–TiO_2/R sample any signal from nitrogen is observed. Its maximum is placed at the position of 396.1 eV, characteristic for metallic nitrides [41]. This position can be associated with the nitride N—Ti—N bond [42] thus proving the substitutional nitrogen doping. Additionally, a small shoulder at the high binding energy side of the N 1s peak is observed. Its position is 398.7 eV and since the presence of titanium oxynitride is suggested above it can represent oxynitride contribution [43,44]

The chemical state of cobalt, iron and nickel additives was also checked by means of XPS. The respective XPS lines for these elements were acquired and they are shown in Fig. 5. The XPS Fe $2p_{3/2}$ line observed for the Fe,N–TiO_2 sample is very broad with the maximum at 710.7 eV (Fig. 5a)). The position of the maximum is characteristic for the presence of Fe^{3+} ions as in Fe_2O_3 or Fe_3O_4 compounds. However, in case of Fe_2O_3 the satellite structure at about 719 eV is expected [45]. Therefore, it is supposed that iron occurs in the studied material in the form of Fe_3O_4 compound. These results stay in accordance with the information revealed by means of XRD method. The position of the maximum of the XPS Co $2p_{3/2}$ line for the Co,N–TiO_2 sample is located at 780.7 eV (Fig. 5b)). The main peak is accompanied by a prominent satellite at 786.7 eV. The position of the main peak as well as the presence of the satellite structure indicate that the cobalt atoms are in oxidized form, likely as octahedrally coordinated, high-spin Co^{2+} oxides, since in case of low-spin octahedrally coordinated Co^{3+} or tetrahedrally coordinated Co^{2+} the satellite structure is not expected [46]. The position of the maximum of XPS Ni $2p_{3/2}$ line for the Ni,N–TiO_2 sample is placed at 855.7 eV (Fig. 5c)). The main peak is accompanied by a prominent satellite at 861.7 eV. The position of the main peak as well as the presence of the satellite structure indicate nickel atoms in oxidized form, likely as Ni^{2+} hydroxides. Moreover, a distinct shoulder at the low energy side of the spectrum can be noticed. It corresponds to the presence of an additional chemical state for which XPS Ni $2p_{3/2}$ is placed at 852.5 eV. This position is characteristic for nickel metal [47]. The presence of this component corroborates the observations of metallic nickel obtained by XRD analysis. It is supposed that during ammonia treatment nickel compounds are partially reduced to Ni^0 state which can be retained even in ambient environment.

Generally, confirming the information about the co-modified materials nature and phase composition delivered by XRD and XPS methods it can be stated with a high probability, that these data are in accordance with each other and that the metal, nitrogen co-modified rutile consists of, as presented in Table 1, mainly titanium dioxide in the form of rutile, and $TiFeO_3$ in case of Fe,N–TiO_2/R, cobalt(II) ions at the Co,N–TiO_2/R photocatalysts

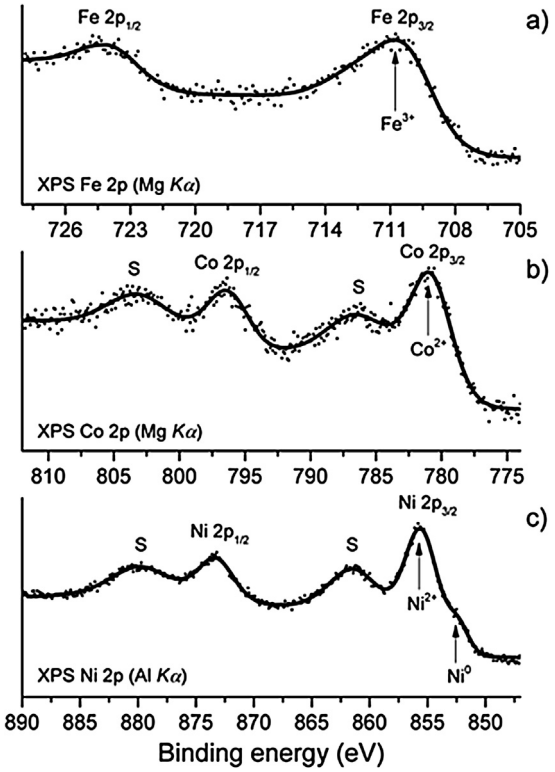

Fig. 5. The XPS spectra of Me $2p_{3/2}$ lines for Me–TiO_2/R photocatalysts. S—denotes satellite.

Table 1
Physicochemical properties of photocatalysts: R—rutile, A—anatase, Am—amorphous.

Properties		Commercial			N–TiO_2	Modified			TiO_2		
		P25	Rutile	TiO_2/A		Fe–TiO_2	Co–TiO_2	Ni–TiO_2	Fe,N–TiO_2	Co,N–TiO_2	Ni,N–TiO_2
Color		White	White	White	Grayish	Brownish	Yellow	Green	Gray–black	Gray–black	Gray–black
Surface concentration (at.%)*	Metal	–	–	–	–	1.1	7.1	2.2	2.1	8.4	2.9
	Nitrogen	–	–	–	6.7	–	–	–	0	0	4
Total Concentration (wt.%)**	Metal	–	–	–	–	4	3.75	4.35	4	3.75	4.25
	Nitrogen	–	–	–	4.8	–	–	–	2.25	0	1.91
S_{BET}(m^2 g^{-1})		55	100	238	16	22	15	16	7	11	20
Phase composition***		R,A	R	A m, A,R	R,TiO_xNy	R, Fe_2O_3	R,$TiCoO_3$	R,$TiNiO_3$	R,$TiFeO_3$	R,Co	R,TiN,Ni

* according to XPS.
** according to ICP-OES.
*** according to XRD.

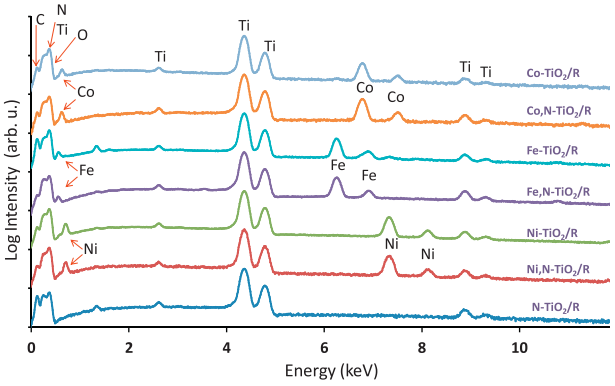

Fig. 6. EDS spectra for Me–TiO_2/R and Me,N–TiO_2/R samples compared with N–TiO_2/R. Note an overlap of N, Ti and O peaks.

surface, and metallic nickel and small amounts of surface TiN phase in case of Ni,N–TiO_2/R material.

In Fig. 6 the spectra collected in EDS analysis are presented. Due to the variation of the current of electron beam typical for cold emission, the total intensity varies with every measurement. Therefore, every spectrum was normalized in respect to the strongest titanium line. Due to the overlap of titanium, oxygen and nitrogen signals it is not possible to discern the nitrogen line from the obtained spectra. Therefore it has to be noted that the presented results do not serve as a proof for nitrogen presence in any of the studied materials. Carbon signal comes from a tape to which the samples were attached. In the spectra, there are well visible *K*α and *K*β signals from cobalt, iron and nickel all of about the same relative Me/Ti intensity ratio. This is in agreement with the ICP–OES measurements (Table 1) from which a correlation between theoretical (5 wt.%) and actual metal concentration in the materials was found. The best agreement between both values was confirmed in case of the nickel-modified materials and the worse in case of the cobalt-modified samples. In Fig. 6 the shift toward higher energies is caused by the increase of atomic number of d block elements of fourth period in the following order Ti, Fe, Co, Ni. In Fig. 7 also the EDS mapping obtained for Co,N–TiO_2/R photocatalysts is additionally presented. Spatial of resolution of EDS technique is about 1 μm and does not allow elemental analysis of nanoparticles visible in Fig. 7. However, EDS mapping confirmed homogeneity of Co,N–TiO_2/R material. Similar results were obtained for all co-modified titanium dioxide (not shown here).

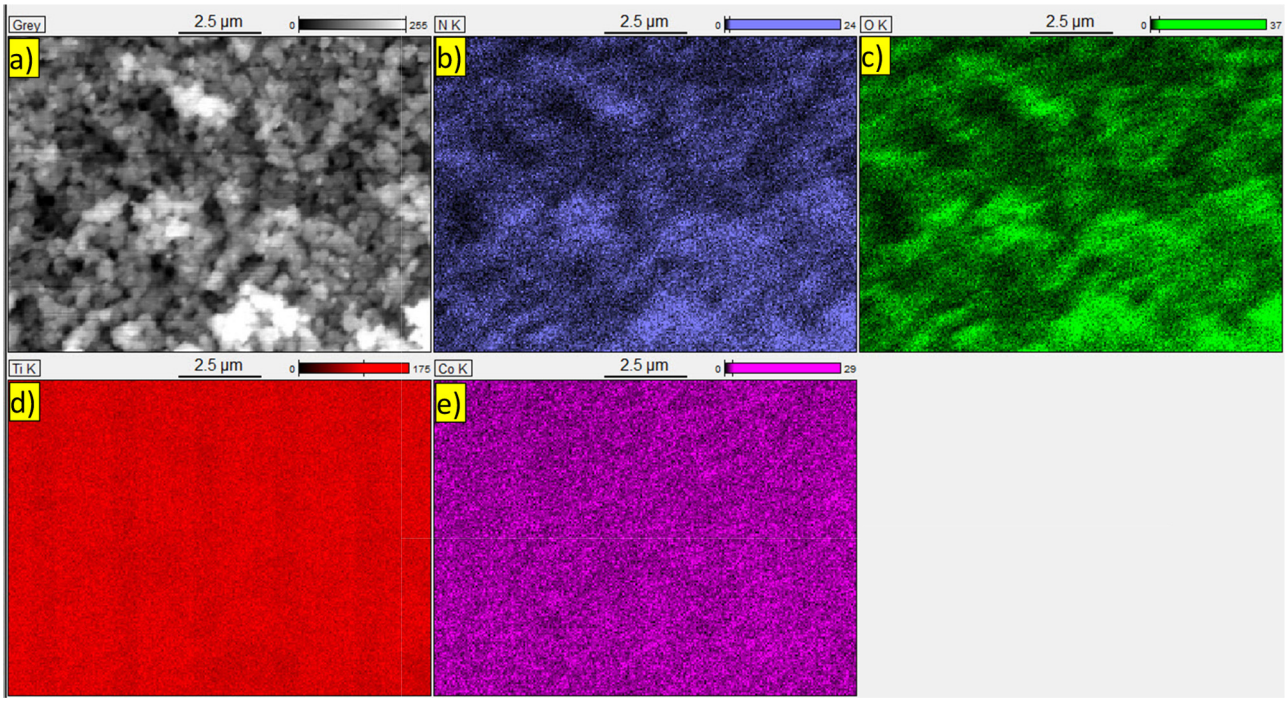

Fig. 7. EDS mapping of Co,N–TiO_2/R sample, distribution of oxygen, titanium, cobalt and nitrogen respectively.

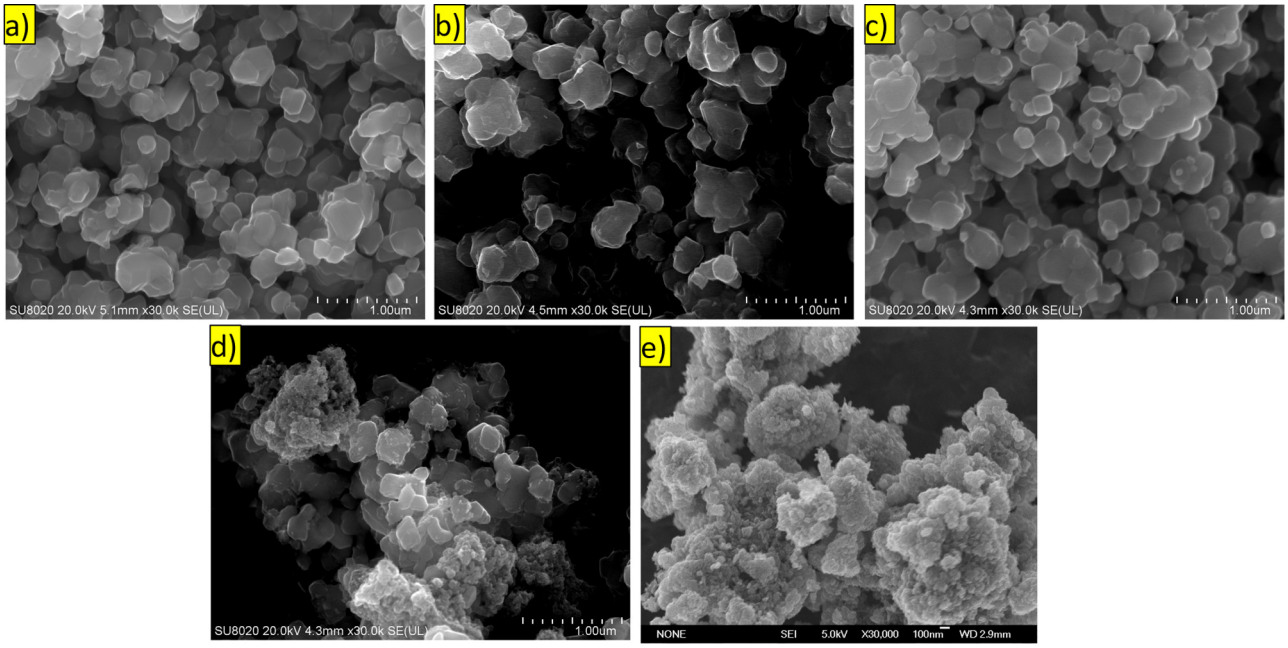

Fig. 8. SEM images of a) Fe,N-TiO2/R; b) Ni,N–TiO_2/R; c) Co,N–TiO_2/R; d) N–TiO_2/R; e) TiO_2/A.

Fig. 8 shows SEM images of TiO_2 after ammonia treatment (a–d) and pristine material (TiO_2/A, (e)) for comparison. In general, the morphology of the samples a–c is similar. The particle size is in range of 100–300 nm. This is a result of sintering of the pristine material (e) at the temperature of 800 °C, which was used during preparation process in order to ensure total transformation of amorphous and anatase phase, present in the starting material, to rutile-TiO_2 form. Titanium dioxide after ammonia treatment but without metal additives (d), consists of two kinds of particles i.e. large ones like in case of other samples and small like in case of pristine TiO_2 (e). This indicates that nitrogen present in TiO_2 lattice may, to some extent, prevent the sintering process. Titanium nitride has much higher melting point than rutile TiO_2, therefore, one may expect that substitution of oxygen ions by nitrogen in TiO_2 lattice will prevent sintering process of small crystals. The sharp SEM images of the nitrided samples were obtained without coating of the sample with a conductive layer. This is not usual for pure titanium dioxide and indicates that all nitrided samples have conducting properties of electric current. In order to confirm the presence of titanium nitride in the N–TiO_2/800 material structure (d), a detailed 48 h XRD measurement was conducted (not shown). The obtained results allowed to detect in the material two phases: rutile and a phase similar to TiN with slight angle shift toward higher values, which suggests lower, than in pure TiN phase, nitrogen concentration. The amount of this phase in the sample is of about 27% and the average crystallite size is 27 nm. These values are in accordance with the information delivered by SEM images.

Another significant difference between the cobalt, nitrogen modified sample in comparison to the iron, nitrogen and nickel, nitrogen materials, besides the much lower concentration of titanium trivalent ions, is the very high surface cobalt concentration (see Table 1). As mentioned, from XPS measurement it was revealed that cobalt at the photocatalyst surface is present in the form of Co^{2+}. Such high concentration of metal ion species on the, already small, surface of the material may limit access of the light photons reaching titanium dioxide and, as a result, suppresses the photocatalytic activity of the material. Note, that the Co^{2+} is present at the surface of the photocatalyst, so any kind of TiO_2 cobalt doping cannot be considered but rather a surface metal ion grafting/decorating effect should be taken into account. Grafting of semiconductors with co-catalysts or metal ions is currently gaining more and more attention of researchers due to the possible charge separation effect, as a result of ion reduction by electrons excited to TiO_2 conduction band. Liu et al. [25,48] described titanium dioxide simultaneously doped and grafted with ions resulting in obtaining visible-light active photocatalysts. For this purpose they used two different metals, namely, iron and copper. What they claimed, was that the photo-excited electron from Fe-doped [47] or Ti^{3+}-doped [48] titanium dioxide conduction band could be transported to the grafted iron or copper ion species at the TiO_2 surface where it was used for metal ion reduction, at the same time decreasing the possibility of e^-/h^+ recombination, thus increasing holes concentration in the valence band of TiO_2 [49,50]. They pointed out in their publications that in order for the metal ions reduction to take place, the energy of photo-excited electron and the metal potential must match. In other words, this means that the photo-excited electron from TiO_2 conduction band must possess more negative potential than the potential required for the grafted ions reduction reaction ($Me^{n+} + ne^- = Me$). In the case of both iron and copper this process was possible since the potential required for their reduction reaction is of 0.77 eV (vs. SHE) and 0.16 eV (vs. SHE), for iron and copper, respectively. Since the potential of electron in TiO_2 conduction band is of about 0 eV, the reduction could take place. However, in case of cobalt the required potential exceeds the electron potential, and unfortunately the metal ion reduction is in this case impossible, since the reduction potential of Co^{2+}/Co couple equals −0.28 eV (vs. SHE) [29]. This means that the cobalt grafted on the photocatalyst surface not only does not cause the increase of charge separation effect, but may even block the titanium dioxide surface and as a result, reduce its activity.

3.4. Photocatalytic Activity

As can be seen in Fig. 9, the visible light activity of all Me–TiO_2/R samples as well as N–TiO_2/R material was similar and comparable to pristine TiO_2/A as well as to commercial photocatalysts' performance. It is worth mentioning here that TiO_2/A sample shows activity in the visible region (400 nm). This phenomenon is

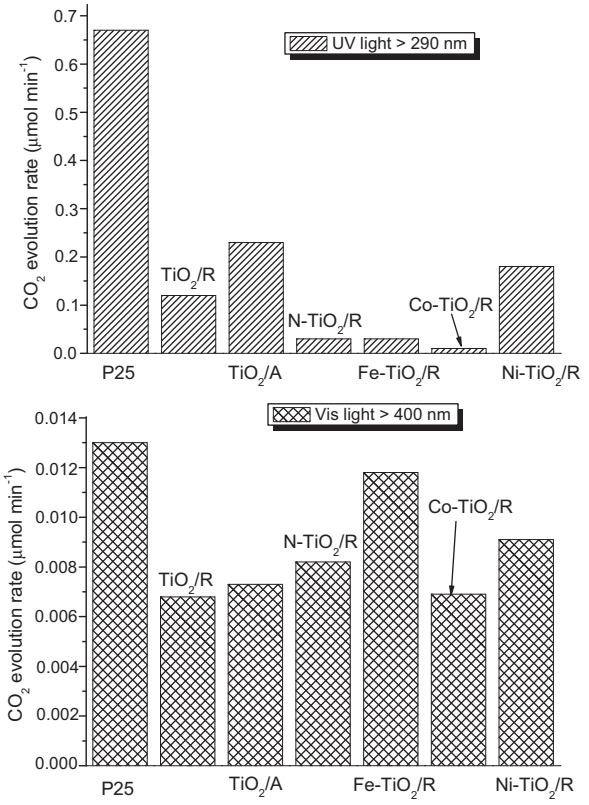

Fig. 9. CO_2 photocatalytic evolution during acetic acid decomposition under UV light (> 290 nm, no cutoff filter) and visible light (>400 nm, with Y42 optical filter) irradiation, in the presence of commercial TiO_2 P25, TiO_2/A and TiO_2 modified with nitrogen or metal.

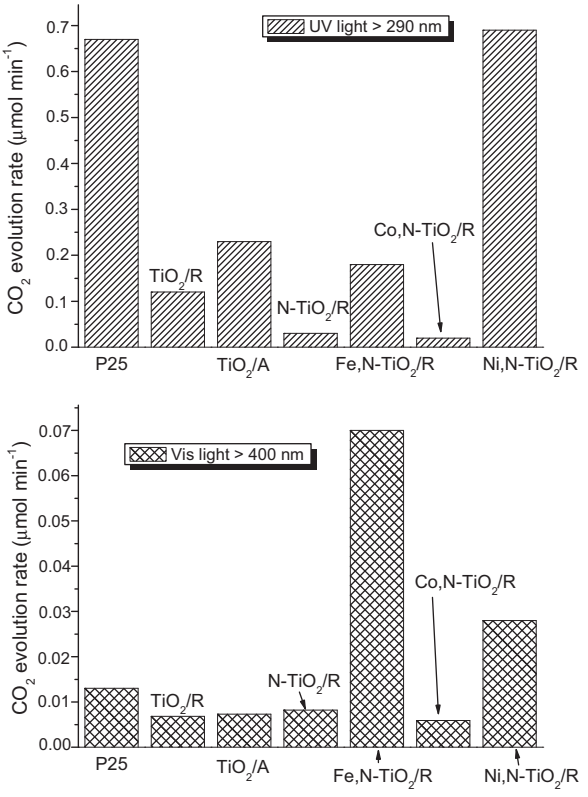

Fig. 10. CO_2 photocatalytic evolution during acetic acid decomposition under UV light (>290 nm, no cutoff filter) and visible light (>400 nm, with Y42 optical filter) irradiation, in the presence of commercial TiO_2 P25, TiO_2/A and TiO_2 modified with nitrogen or co-modified with nitrogen and metal.

possible due to small content of rutile phase in this sample (see Section 2) as well as the presence of residual sulfur in its structure, which may extend absorption of TiO_2/A towards longer wavelengths. At the same time the UV light activity of all modified samples is significantly lower than that of commercially available materials. This means that these kinds of photocatalytic junctions are able to utilize visible light for photocatalytic purposes, nevertheless, their activity is rather low. The explanation of these phenomena may be as follows: excited electrons from conduction band of TiO_2 may be transported to the conduction band of $TiFe_2O_5$, $CoTiO_3$ or $NiTiO_3$ due to its advantageous, more positive potential [29]. However, this potential is simply too positive and electrons from this position cannot take part in hydroxyl radicals creation via oxygen reduction and/or water reduction processes. At the same time, electrons from the valence band of $TiFe_2O_5$, $CoTiO_3$ and $NiTiO_3$ may be transferred towards titanium dioxide valence band, also due to potentials differences. In this way, holes from TiO_2 valence band undergo recombination, whereas in the ternary metal oxides the valence bands holes are being created. Since the valence band potential of the newly formed holes in $TiFe_2O_5$, $CoTiO_3$ and $NiTiO_3$ is more negative than the potential of the hole in TiO_2 valence band it is less likely that the former holes will take part in the direct acetic acid oxidation [19]. This means that in this case a typical trade-off takes place, i.e. the semiconductors' coupling increases charge separation, but at the same time, the potential of electrons and holes becomes less advantageous for photocatalytic redox reactions to occur. What is more, due to high temperature applied during preparation process, the material underwent sintering leading to the formation of large, well defined rutile crystals, with small surface areas, which may cause significant deterioration of the photocatalytic performance of TiO_2 [33]. Both visible and UV light photocatalytic activity seem to depend on the employed metal (Me) and were the highest for iron and nickel modified rutile TiO_2, respectively. In case of the co-modified samples, the differences between materials with various metals applied for the modification are much more significant, both in respect to their physicochemical properties and photocatalytic activity. In Fig. 10 the photocatalytic activity results for all the co-modified materials (Me,N–TiO_2/R) together with N-doped TiO_2 (N–TiO_2/R), the starting titanium dioxide (TiO_2/A), commercial P25 and TiO_2/R for comparison purpose, under two types of irradiation are presented. It can be seen that the photocatalytic activity of the cobalt,nitrogen co-modified rutile is, as expected, rather low, under both UV and visible light irradiation. This may be due to the earlier described phenomena: low surface area and additionally large amounts of cobalt ions at the surface limit the number of photons which are able to take part in the materials' excitation process, which may cause a deterioration of visible light activity of this material in respect to other co-modified samples. Moreover, as argued, the Co^{2+} ions at the TiO_2 surface do not take part in the charge separation processes. Additionally, the presence of small amounts of trivalent titanium ions in the structure of the photocatalyst may even increase the recombination rate of the photogenerated charges and thus the overall photocatalytic performance of these materials remains unsatisfying. This situation is different from the case of the iron,nitrogen co-modified and nickel,nitrogen co-modified materials. The totally different photocatalytic performance of these materials derives from their drastically different physicochemical properties. The high activity of the nickel,nitrogen co-modified sample may derive, as described in our previous publication, from a few aspects: (a) rutile form of TiO_2, which assures better stability and light absorption ability than anatase or amorphous TiO_2; (b) doped nitrogen and presence of Ti^{3+} ions in the photocatalyst structure, mainly in the

bulk of TiO_2, which allows visible light absorption by narrowing the band-gap of the material, additionally increasing TiO_2 stability but not yet serving as hole trap and therefore not inhibiting the photocurrent; (c) nickel modification, resulting in significant amounts of nickel on the photocatalysts' surface as well as in the bulk, which may form Schottky barrier at the materials' surface allowing effective electron transfer from TiO_2 conduction band (or electrons from new energy states created due to high Ti^{3+} concentration) towards metallic nickel, thus improving significantly charge separation; (d) presence of TiN on TiO_2 surface, which may also serve as an electron trap and increase the charge separation. As can be noticed, also the results obtained for Fe,N–TiO_2/R revealed an excellent increase in the visible light photoactivity of the co-modified sample, in comparison with the starting material (TiO_2/A) as well as the commercial photocatalysts. This dramatic visible light activity increase was ascribed to the synergistic effect of the Fe,N rutile co-modification. The combination of doped nitrogen and a presence of titanium trivalent ions caused a band-gap narrowing allowing absorption of longer wavelengths from visible light region, whereas iron in the form of $FeTiO_3$ allowed to increase the efficiency of charge separation by means of the inter-phase electron transport from TiO_2 conduction band/defects energy state to Fe_2O_3 conduction band. Moreover, in the contrary to Fe–TiO_2/R material, the charge transfer between the semiconductors' valence bands is rather impossible due to very similar potentials. Thus, the potential of the holes photogenerated in the titanium dioxide valence band was sufficiently high for acetic acid direct oxidation. As a result, a significantly improved photocatalytic performance of the materials was observed. The obtained results lead to a conclusion that in case of both nickel,nitrogen co-modified material and iron,nitrogen co-modified material the electron transfer processes are similar, resulting in significant improvement of the visible light activity of these materials. Nitrogen and Ti^{3+} species allow absorption of a wide light spectrum and the presence of Fe_2O_3 or Ni/TiN at the photocatalysts' surface facilitates effective charge transfer, inhibiting the e^-/h^+ recombination. However, the visible light performance of Ni,N–TiO_2/R is significantly lower than that of Fe,N–TiO_2/R. Moreover, only in case of the nickel,nitrogen co-modified material, except from its high visible light performance, one can also observe a significant improvement of the photoactivity of this material in the UV region. The higher visible light activity of Fe,N–TiO_2/R in regard to Ni,N–TiO_2/R may derive from the following properties of this material: (a) the presence of the coupled $FeTiO_3$ semiconductor with lower band gap, which may increase the major charge carrier concentration in this material via light absorption/excitation mechanism, resulting in higher photocurrent density. Higher electron/hole pairs density increases the possibility of a photocatalytic reaction on the materials surface; (b) the lack of metal impurities on the photocatalysts surface. The presence of impurities in TiO_2 structure may be beneficial for the light absorption properties of this material, nevertheless, it may also serve as a recombination center. In case of nanoparticles the bulk transport resistance is less pronounced than in case of films or bulk photocatalysts, at the same time the surface of the material and the kinetics of charge transfer from the semiconductor surface to a contaminant in the solution or adsorbed on its surface becomes crucial and may be a limiting factor for the photocatalytic activity of these materials. Lack of impurities at the TiO_2 surface, which may either block adsorption of contaminants on TiO_2 or/and decrease light absorption coefficient of the material due to reflecting visible light and which may also serve as a charge recombination center, may be a key factor responsible for such high visible light performance of Fe,N–TiO_2/R photocatalyst. On the other hand only in case of the nickel,nitrogen co-modified material, except from its high visible light performance, one can also observe a dramatic improvement of the photoactivity of this material in the UV region. This increase derives, most probably, from the presence of metallic nickel at the semiconductor surface, which may lead to a plasmonic excitation of metal. Surface plasmon effect is well known to cause a significant increase of semiconductors' photocatalytic activity, due to the collective oscillations of the electrons at the surface of the nanoparticles which causes plasmon resonance [51]. Upon irradiation, the valence electrons in a (noble) metal nanoparticle undergo a collective oscillatory motion. This phenomenon, called surface plasmon resonance (SPR), can enhance the charge density in the semiconductors by several mechanisms, namely (a) plasmon resonance energy transfer (PRET) [52], known also as the near-field mechanism; this mechanism is only possible if light absorption spectra of metal nanoparticles overlap with semiconductors absorption spectra; (b) hot electron injection [53], which can occur only if the energy of the hot electron/hole is larger than the energy of Schottky barrier formed at the nanoparticle-semiconductor interface, and/or (c) light scattering, which may take place if the refractive index of a semiconductor is higher than the refractive index of the surrounding solvent—light is always scattered into the material with a larger refractive index. Since in case of the semiconductor-water interface this is practically always the case, the light scattering is a very common effect of surface nanoparticles interaction with semiconductors.There are numerous papers available discussing the possibility of plasmonic functionalization of TiO_2 [54,55]. Zaleska et al. [56] prepared Au–TiO_2 and Ag/Au–TiO_2 nanoparticles using a water-in-oil micro-emulsion system. They confirmed the increased visible light activity of titanium dioxide surface modified with gold and/or silver nanoparticles, they also found that the best photocatalytic activity revealed samples with large gold particles (~90 nm) deposited on small titania nanoparticles. Tsukamoto et al. [57] functionalized commercial P25 with gold nanoparticles with diameter below 5 nm. The gold nanoparticles were located at the interface of anatase/rutile TiO_2 particles. They claimed that plasmon activation of the Au particles by visible light was followed by hot electron injection between Au and rutile/anatase contact site, resulting in enhanced photocatalytic activity of this system. As reported by Filippov et al. [58], the appearance of the local surface plasmons excitation is also possible in the Ni shell but, as they pointed out in their recent paper from 2013 [59], in contrary to the more extensively studied noble metals (Ag, Au), in case of nickel the plasmonic effect is only realized under UV light irradiation. As an evidence for plasmonic effect on nickel nanoparticles they provided the time-resolved photoluminescence (PL) measurements [59]. The presented here results suggest contribution of UV light plasmonic surface effect of nickel particles formed at TiO_2 surface to the UV-light activity.

4. Conclusions

In summary, this study demonstrate a new and simple method for the synthesis of Me-modified, N-doped and Me,N-co-modified rutile-TiO_2 photocatalysts. Detailed physicochemical properties and photocatalytic activity investigations were conducted in order to feature the influence of the applied modification procedure on their properties and to shed light on the origin of rutile UV and visible light activity.

The presented studies show that metal-modified rutile TiO_2 as well as nitrogen-doped rutile TiO_2 are photocatalytically active, however, their performance is rather poor under applied conditions. It was proven, though, that proper co-modification of rutile titanium dioxide may lead to obtaining materials exhibiting high visible (Fe,N–TiO_2/R) or UV light photocatalytic activity (Ni,N–TiO_2/R). The photocatalytic activity and physicochemical properties of these materials strongly depend on the metal applied during the impregnation step. It was shown that doped nitrogen

and the presence of Ti^{3+} ions in TiO_2 structure cause significant improvement of visible light absorption of TiO_2 by narrowing its band gap, whereas the presence of proper amount and form of metal on titanium dioxide surface facilitates electron/hole pairs separation. Combination of these two effects causes a significant improvement of photocatalytic activity of the materials. Moreover, in case of nickel, nitrogen co-modified samples the dramatic increase of UV light activity has been ascribed to the surface plasmon excitation of metallic nickel. Finally, it was shown that cobalt and cobalt, nitrogen TiO_2-modification did not cause improvement of photocatalytic performance of titanium dioxde neither under visible nor UV light irradiation.

Acknowledgments

This work was supported by National Centre for Science and Ministry of Science and Higher Education of Poland decision number 802/N-JAPONIA/2010/0 under project No. MNiSW/DPN/4878/TD/2010. The authors would like to thank Professor Barbara Grzmil from West Pomeranian University of Technology, Szczecin for helpful assistance during XRD measurements.

Appendix A. Supplementary data

Supplementary material related to this article can be found, in the online version, at http://dx.doi.org/10.1016/j.apcatb.2014.07.001.

References

[1] M. Radetić, J. Photochem. Photobiol., C: Photochem. Rev. 16 (2013) 62–76.
[2] S. Ahmed, M.G. Rasul, W.N. Martens, R. Brown, M.A. Hashib, Desalination 261 (2010) 3–18.
[3] M. Batzill, E.H. Morales, U. Diebold, Phys. Lett. Rev. 96 (2006) 026103.
[4] N. Serpone, J. Phys. Chem. B 110 (2006) 24287–24293.
[5] Shigeru Ikeda, N. Sugiyama, B. Pal, G. Marcí, L. Palmisano, H. Noguchi, K. Uosaki, B. Ohtani, Phys. Chem. Chem. Phys. 3 (2001) 267–273.
[6] I.A. Shkrob, M.C. Sauer Jr., J. Phys. Chem. B 108 (2004) 12497–12511.
[7] B. Ohtani, R.M. Bowman, D.P. Colombo Jr., H. Kominami, H. Noguchi, K. Uosaki, Chem. Lett. 27 (1998) 579–580.
[8] A. Fujishima, T.N. Rao, D.A. Truk, J. Photochem. Photobiol., C: Photochem. Rev. 1 (2000) 1.
[9] S.H. Cheung, P. Nachimuthu, A.G. Joly, M.H. Engelhard, M.K. Bowman, S.A. Chambers, Surf. Sci. 601 (2007) 1754–1762.
[10] J.A. Navio, M. Macias, M. Gonzales-Catalan, A. Justo, J. Mat. Sci. 27 (1992) 3036–3042.
[11] A. Heciak, A.W. Morawski, B. Grzmil, S. Mozia, Appl. Catal., B: Environ. 140–141 (2013) 108–114.
[12] Y. Wang, R. Shi, J. Lin, Y. Zhu, Appl. Catal., B: Environ. 100 (2010) 179–183.
[13] Z. Liu, D. He, Y. Wang, H. Wu, J. Wang, Synth. Met. 160 (2010) 1036–1039.
[14] M.A. Ahmed, E.E. El-Katori, Z.H. Gharni, J. Alloys Compd. 553 (2013) 19–29.
[15] S. Ch. Lan, W.N. Kai, I. Shaliza, S. Pichiah, Int. J. Photoenergy 2013 (2013) 10 (Article ID 659013).
[16] R. Asahi, T. Morikawa, T. Ohwaki, K. Aoki, Y. Taga, Science 293 (2001) 269–271.
[17] M.V. Dozzi, E. Selli, J. Photochem. Photobiol., C: Photochem. Rev. 14 (2013) 13–28.
[18] M. Pelaez, N.T. Nolan, S.C. Pillai, M.K. Seery, P. Falaras, A.G. Kontos, P.S.M. Dunlop, J.W.J. Hamilton, J.A. Byme, K. O'Shea, M.H. Entezari, D.D. Dionysiou, Appl. Catal., B: Environ. 125 (2012) 331–349.
[19] J.A. Rengifo-Herrera, K. Pierzchała, A. Sienkiewicz, L. Forro, J. Kiwi, C. Pulgarin, Appl. Catal., B: Environ. 88 (2009) 398–406.
[20] C.D. Valentin, G. Pacchioni, A. Selloni, Phys. Rev. B: Condens. Matter 70 (2004) 085116.
[21] C. Di Valentin, A. Selloni, S. Livraghi, M.C. Paganini, E. Giamello, Chem. Phys. 339 (2007) 44–56.
[22] C. Creutz, B.S. Brunschwig, N.J. Suntin, Phys. Chem. B 109 (2005) 10251–10260.
[23] N.S.J. Hush, Electrochim. Acta 13 (1968) 1005–1023.
[24] N.S.J. Hush, Electroanal. Chem. 470 (1999) 170–195.
[25] M. Liu, X. Qiu, M. Miyauchi, K. Hashimoto, J. Am. Chem. Soc. 135 (2013) 10064–10072.
[26] D. Dolat, S. Mozia, B. Ohtani, A.W. Morawski, Chem. Eng. J. 225 (2013) 358–364.
[27] D. Dolat, B. Ohtani, S. Mozia, D. Moszynski, N. Guskos, Z. Lendzion-Bielun, A.W. Morawski, Chem. Eng. J. 239 (2014) 149–157.
[28] D. Dolat, N. Quici, E. Kusiak-Nejman, A.W. Morawski, G. Li Puma, Appl. Catal., B: Environ. 115 (2012) 81–89.
[29] D.R. Lide, CRC Handbook of Chemistry and Physics, CRC, Boca Raton, FL, 2009.
[30] S. Sivakumar, A. Selvaraj, A.K. Ramasamy, V. Balasubramanian, Water, Air, Soil Pollut. 224 (2013) 1529.
[31] R. Pärna, U. Joost, E. Nõmmiste, T. Käämbre, A. Kikas, I. Kuusik, M. Hirsimäki, I. Kink, V. Kisand, Appl. Surf. Sci. 257 (2011) 6897–6907.
[32] P.N. Kapoor, S. Uma, S. Rodriguez, K.J. Klabunde, J. Mol. Catal., A: Chem. 229 (2005) 145–150.
[33] S. Mozia, K. Bubacz, M. Janus, A.W. Morawski, J. Hazard. Mater. 203–204 (2012) 128–136.
[34] F. Teng, M. Li, C. Gao, G. Zhang, P. Zhang, Y. Wang, L. Chen, E. Xie, Appl. Catal., B: Environ. 148–149 (2014) 339–343.
[35] A. Naldoni, M. Allieta, S. Santangelo, M. Marelli, F. Fabbri, S. Cappelli, C.L. Bianchi, R. Psaro, V. Dal Santo, J. Am. Chem. Soc. 134 (2012) 7600–7603.
[36] J. Weidmann, Th. Dittrich, E. Konstantinova, I. Lauermann, I. Uhlendorf, F. Koch, Sol. Energy Mater. Sol. Cells 56 (1999) 153–165.
[37] P.-F. Chauvy, P. Hoffmann, D. Landolt, Appl. Surf. Sci. 211 (2003) 113–127.
[38] Y. Cong, J. Zhang, F. Chen, M. Anpo, J. Phys. Chem. C 111 (2007) 6976–6982.
[39] J. Wang, W. Zhu, Y. Zhang, S. Liu, J. Phys. Chem. C 111 (2007) 1010–1014.
[40] D. Dolat, D. Moszyński, N. Guskos, B. Ohtani, A.W. Morawski, Appl. Surf. Sci. 266 (2013) 410–419.
[41] J.F. Moulder, W.E. Stickle, P.E. Sobol, K.E. Bomben, Handbook of X-ray Photoelectron Spectroscopy, Perkin-Elmer, Eden Prairie, MN, 1992.
[42] A. Manole, V. Dăscăleanu, M. Dobromir, D. Luca, Surf. Interface Anal. 42 (2010) 947–954.
[43] A. Rizzo, M.A. Signore, L. Mirenghi, T. Di Luccio, Thin Solid Films 517 (2009) 5956–5964.
[44] Y. Wu, H. Liu, J. Zhang, F. Chen, J. Phys. Chem. C 113 (2009) 14689–14695.
[45] T. Yamashita, P. Hayes, Appl. Surf. Sci. 254 (2008) 2441–2449.
[46] S.C. Petitto, E.M. Marsh, G.A. Carson, M.A. Langell, J. Mol. Catal., A: Chem. 281 (2008) 49–58.
[47] J.C. de Jesus, J. Carrazza, P. Pereira, F. Zaera, Surf. Sci. 397 (1998) 34–47.
[48] M. Liu, X. Qiu, M. Miyauchi, K. Hashimoto, Chem. Mater. 23 (2011) 5282–5286.
[49] H. Yu, H. Irie, Y. Shimodaira, Y. Hosogi, Y. Kuroda, M. Miyauchi, K. Hashimoto, J. Phys. Chem. C 114 (2010) 16481–16487.
[50] S.B. Rawal, H.J. Kim, W.I. Lee, Appl. Catal., B: Environ. 142–143 (2013) 458–464.
[51] Y. Tian, T. Tatsum, J. Am. Chem. Soc. 127 (2005) 7632–7637.
[52] D.B. Ingram, S. Linic, J. Am. Chem. Soc. 133 (2011) 5202–5205.
[53] Y. Tian, T. Tatsuma, J. Am. Chem. Soc. 127 (2005) 7632–7637.
[54] H. Wang, T. You, W. Shi, J. Phys. Chem. C 116 (10) (2012) 6490–6494.
[55] S.T. Kochuveedu, D. Kim, D. Kim, J. Phys. Chem. C 116 (3) (2012) 2500–2506.
[56] A. Zielińska-Jurek, E. Kowalska, J.W. Sobczak, W. Lisowski, B. Ohtani, A. Zaleska, Appl. Catal., B: Environ. 101 (2011) 504–514.
[57] D. Tsukamoto, Y. Shiraishi, Y. Sugano, S. Ichikawa, S. Tanaka, T. Hirai, Am. Chem. Soc. 134 (14) (2012) 6309–6315.
[58] S. Filippov, X.J. Wang, M. Devika, N. Koteeswara Reddy, C.W. Tu, W.M. Chen, I.A. Buyanova, J. Appl. Phys. 113 (2013) 214302–214308.
[59] Q.J. Ren, S. Filippov, S.L. Chen, M. Devika, N. Koteeswara Reddy, C.W. Tu, W.M. Chen, I.A. Buyanova, Nanotechnology 23 (2012) 4252–42501.